Acta Materialia 248 (2023) 118797

Contents lists available at ScienceDirect

Acta Materialia

journal homepage: www.elsevier.com/locate/actamat

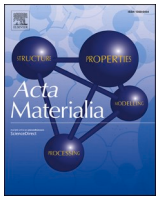

# Twin suppression by atomic scale engineering of precipitate-matrix interfaces

X.Z. Jin [a], C.Y. Wang [b], S. Milenkovic [a], I. Sabirov [a], I.J. Beyerlein [c], M.T. Pérez-Prado [a,*]

[a] IMDEA Materials Institute, C/ Eric Kandel, 2, Getafe, Madrid 28906, Spain
[b] State Key Laboratory of Solidification Processing, Northwestern Polytechnical University, Xi'an 710072, China
[c] Department of Mechanical Engineering and Materials, University of California, Santa Barbara, CA 93101, USA

ARTICLE INFO

*Keywords:*
Magnesium
Atomic scale engineering
Precipitate-matrix interface
Segregation
Twinning

ABSTRACT

This work aims to investigate the influence of solute segregation at particle-matrix interfaces on the twin activity of aged Mg alloys. With that purpose a binary Mg-8Al alloy (wt%) and two ternary Mg-8Al-1 Zn and Mg-8Al-1Ag alloys (wt%) were first homogenized and then aged in order to obtain comparable precipitate distributions. Particle-matrix interfaces in the binary alloy were observed to be clean, while Zn and Ag atomic segregation was clearly present at the interfaces of the ternary alloys. Room temperature micropillar compression tests were carried out in grains with favorable orientations for tensile twinning in the homogenized and the aged conditions for the three materials under investigation. The activation of twinning and slip was then characterized by electron microscopy. This study shows that while in the binary alloy precipitation did not lead to any major changes in the twinning activity and, in particular, it did not prevent the formation of thick twin lamellae encompassing the entire width of the tested micropillars, a drastic reduction of the twin activity took place in the aged ternary alloys. In the latter, straining led to the formation of narrow twin lamellae belonging to a single variant, and occasionally arrested at the interior of the micropillars. We propose that the drastic reduction of the twin volume fraction in the aged ternary alloys may be attributed to the decrease of the particle-matrix interface energy due to Zn and Ag segregation, which would hinder re-nucleation at such interfaces, thus suppressing twin propagation.

## 1. Introduction

Vehicle light weighting is a well-known strategy to enhance sustainable mobility, especially in the case of electric transport, where a reduction in weight can result in lower charging times, in longer autonomy, or in the need for smaller batteries [1–2]. Magnesium (Mg) alloys, owing to their low density and high specific strength, are envisioned to have great potential to contribute to improve energy efficiency [3–5]. Furthermore, they are endowed with good recyclability, a fact that enhances their eco-friendly nature. Structural applications of Mg alloys in automotive remain, however, restricted by some limiting mechanical properties that are inherent to their hexagonal close packed (hcp) lattice, including low strength in comparison with steel or high strength Al alloys, low temperature mechanical anisotropy and yield asymmetry and, additionally, susceptibility to corrosion [6].

Despite the tremendous efforts that have been devoted over the past two decades towards understanding the physical metallurgy of Mg alloys [7–9], in an attempt to improve their overall mechanical response, some fundamental questions remain unanswered. For example, it is still not clear how to fully suppress twinning in {10–12} planes, a relatively soft mechanism that contributes to the limited strength of many alloy systems, to the anisotropic mechanical behavior and, in particular, to the strong tension-compression yield asymmetry in wrought alloys, which limits severely their formability [10–13].

Several methods aimed at reducing the activation of twinning have been put forward [14]. On the one hand, texture weakening has been attempted by alloying with a combination of rare-earth (RE) elements, such as cerium (Ce), gadolinium (Gd), niobium (Nb), or ytrium (Y), and with other large elements such as calcium (Ca) [15–18], by the use of processing methods such as twin roll casting [19], or by a combination of both. Due to the twin polarity, the activity of twinning during compression of weakly textured alloys is significantly smaller than that present in wrought conventional alloys, which are commonly endowed with strong textures. However, RE elements are critical raw materials

* Corresponding author.
*E-mail address:* teresa.perez.prado@imdea.org (M.T. Pérez-Prado).

https://doi.org/10.1016/j.actamat.2023.118797
Received 12 September 2022; Received in revised form 16 February 2023; Accepted 17 February 2023
Available online 23 February 2023

with a large environmental footprint and thus their use is becoming increasingly less desirable. On the other hand, twin hardening has been attempted by RE solid solution [20], by grain refinement [21], and by precipitation [22,23]. None of these strategies have, however, succeeded to completely suppress twinning.

Increasing the strengthening effect of precipitation on twinning requires a thorough understanding of the complex interactions between precipitates and twins [24] which is, to date, still lacking. Twinning proceeds by the nucleation, propagation and growth of irregular, three-dimensional domains [25] that develop by a combination of lattice shear and atomic shuffling [26]. Precipitates reportedly hinder mostly the propagation stage, preventing twin growth, but they either do not have a strong effect on twin nucleation [27–30], or they even stimulate it [31]. Thus, twins in aged Mg alloys are usually narrow and large in number [24,27,29–33]. Twinning is, in general, strengthened by precipitation [27,29–35], with the exception of some Mg-RE alloys, where solid solution strengthening is very potent, and where thus aging reportedly gives rise to twin softening with respect to the solid solution state [36]. The changes induced in a given precipitate as a consequence of the passage of a twin boundary include, in most cases, a small elastic rotation of the particle lattice [18,27,29,34,35], but also particle twinning [18], particle dissolution [37], or particle shearing [38]. It has been reported that the specific interaction mechanism is a function of the precipitate size [32,39,40] and of the nature of the twin boundary segment (whether it is coherent or if it is an intersection between a coherent segment and a prismatic-basal or basal-prismatic segment) [41–43]. In general, the overall twin volume fraction in aged alloys is not dramatically altered with respect to the solid solution state. Twin suppression, which is essential for the elimination of the yield asymmetry in Mg alloys and, in general, for the reduction of their mechanical anisotropy in the absence of RE alloying additions, requires the presence of newly engineered precipitates that can constitute more effective obstacles for twin propagation and growth.

The aim of this work is to investigate the effect of atomic segregation at the precipitate-matrix interface on twin propagation. With that aim, a binary Mg-8 wt% Al alloy and two ternary Mg-8 wt% Al-1 wt% Zn and Mg-8 wt% Al-1 wt% Ag alloys were prepared by casting and hot compression, and the three were peak aged to develop a homogeneous distribution of $Mg_{17}Al_{12}$ (b) precipitates. Zinc and silver were selected as ternary alloying additions because of their known tendency to segregate at $Mg_{17}Al_{12}$–Mg interfaces. The influence of Zn and Ag interfacial atomic segregation on the twin volume fraction was investigated using an experimental approach including micromechanical testing and transmission electron microscopy. This work provides new guidelines for atomic scale engineering of precipitates that can effectively prevent twin propagation in Mg alloys.

## 2. Experimental procedure

The materials investigated in the present study were a binary reference alloy with the composition of Mg-8 wt.% Al (hereafter termed Mg-Al), and two ternary alloys with compositions Mg-8 wt% Al-1 wt%Zn and Mg-8 wt% Al-1 wt%Ag (hereafter termed Mg-Al-Zn and Mg-Al-Ag). Zinc and silver were selected as the ternary alloying additions because they are known to segregate to precipitate-matrix interfaces in aged Mg alloys [44,45]. Rods of these three alloys, with a diameter of 10 mm and a length of 100 mm, were cast in an induction furnace (VSG 002 DS, PVA TePla) under the protection of an Ar atmosphere using the pure Mg, Al, Zn and Ag elements as raw materials. The as-cast alloys were then solid solution treated at 420 °C for 15 h, and then they were compressed at 380 °C with a constant speed of 1 mm/min to a strain of 50% to reduce the microstructural defects resulting from the casting process. Next, in order to generate a large grain size that could allow to minimize the effect of grain boundaries on micromechanical tests, the compressed samples were homogenized at 420 °C for 15 h and quenched in water [46]. This state will be termed the “homogenized condition” and it is well known that the resulting alloys are solid solutions. An aging study was then performed in order to find peak aging conditions for the three alloys. It was found that aging at 200 °C for 15 h led to maximum hardness in all the materials investigated. Therefore, peak aging was

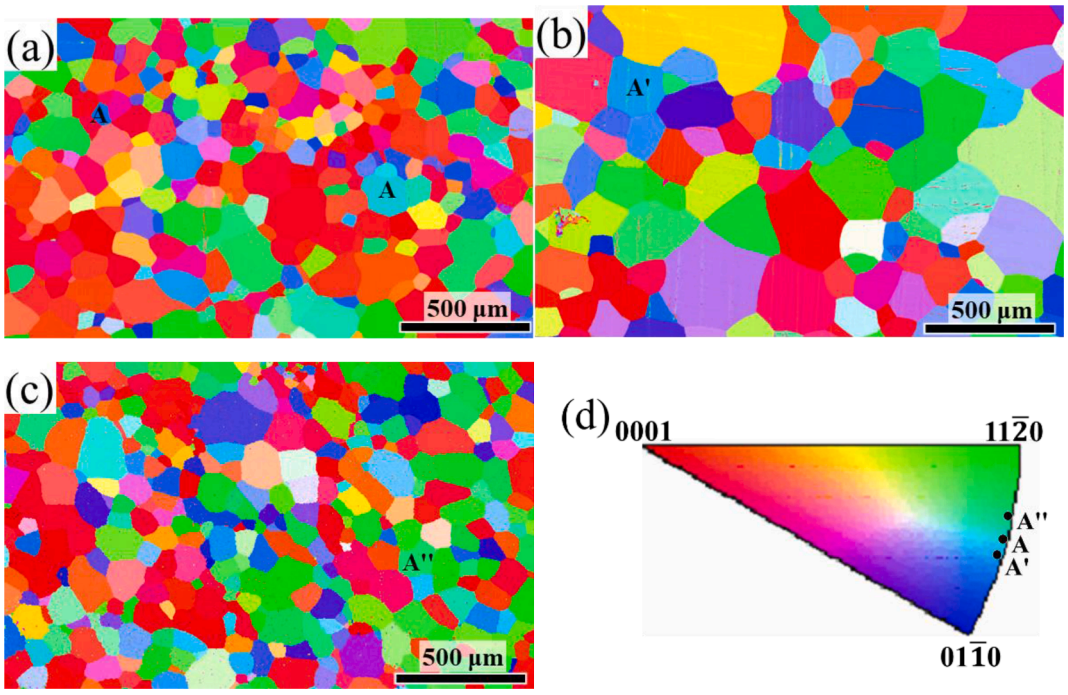


**Fig. 1.** EBSD inverse pole figure maps in the direction normal to the surface of the homogenized polycrystalline Mg alloys: (a) Mg-8 wt% Al, (b) Mg-8 wt%Al-1 wt% Zn, (c) Mg-8 wt%Al-1 wt% Ag. The grains selected for micropillar compression, named, respectively, A, A′, and A″, are highlighted in bold letters in each map. (d) Inverse pole figure showing the orientation of the normal to the surface (parallel to the compression axis in the corresponding micropillar compression tests) in the selected grains, as well as the color coding for the EBSD inverse pole figure maps.

**Table 1**
Euler angles ($\varphi_1$, $\phi$, $\varphi_2$) and Schmid factors (SFs) corresponding to basal ($SF_{basal}$), prismatic ($SF_{prism}$), and {11–22} pyramidal ($SF_{pyr}$) slip, as well as to tensile twinning ($SF_{twin}$) of the grains selected for the micromechanical study in the homogenized and aged alloys.

| Alloy | Mg-Al | | Mg-Al-Zn | | Mg-Al-Ag | |
|---|---|---|---|---|---|---|
| Condition | Homogenized | Aged | Homogenized | Aged | Homogenized | Aged |
| Grain | A | B | A' | B' | A'' | B'' |
| Euler angles (°) ($\varphi_1$, $\phi$, $\varphi_{22}$) | (90, 88.3, 45.4) | (10.0, 88.8, 45.5) | (90, 88.9, 17.1) | (0, 92.3, 45.4) | (62.9, 88.4, 10.7) | (90.0, 92.7, 45.2) |
| α (°) | 88.3 | 88.8 | 87.9 | 87.7 | 88.4 | 87.3 |
| $SF_{basal}$ | 0.03 | 0.02 | 0.01 | 0.03 | 0.03 | 0.05 |
| $SF_{prism}$ | 0.50 | 0.50 | 0.50 | 0.50 | 0.49 | 0.49 |
| $SF_{twin}$ | 0.46 | 0.46 | 0.47 | 0.46 | 0.44 | 0.47 |
| $SF_{pyr}$ | 0.43 | 0.43 | 0.42 | 0.43 | 0.44 | 0.44 |

Note: α represents the angle between the micropillar compression axis and the crystal c-axis of Mg alloy.

performed at 200 °C for 15 h to induce the precipitation of the $Mg_{17}Al_{12}$ particles, which are the hardening phase in the Mg-Al system [46]. This state will be termed the "aged condition".

The microstructure of the homogenized and aged alloys was examined first by electron backscatter diffraction (EBSD) using a voltage of 20 kV, a beam current of 2.7 nA, and a step size of 1 mm in a field emission gun (FEG) SEM (Helios NanoLab 600i, FEI) equipped with an HKL detector, a charged coupled device camera, as well as dedicated softwares for data acquisition and data analysis (Aztec and Channel 5.0, respectively). Sample preparation for EBSD acquisition consisted of grinding with SiC papers of increasingly smaller grit size, mechanical polishing with diamond suspensions containing different particle sizes, and surface finishing using a colloidal silica slurry. The distribution of precipitates in the aged alloys was examined by bright field scanning transmission electron microscopy (BF-STEM) along the $<11-20>_\alpha$ zone axis (ZA) and by regular bright field TEM along the $<0001>_\alpha$ zone axis on a FEI Talos F200x microscope using a voltage of 200 kV. Atomic segregation at precipitate-matrix interfaces was analyzed by high resolution scanning transmission electron microscopy (HR-STEM) along the ⟨11–20⟩ zone axis using a probe-corrected FEI Titan 60–300 microscope operated at 300 kV and equipped with a high brightness X-FEG and a Cs CETCOR corrector for the condenser system to provide sub-angstrom probe size. Selected area diffraction (SAD) was utilized to verify the orientation of the lattice within the twinned regions. The lamellae were extracted using the FIB-lift-out technique and then milled to a thickness of ~100 nm using the focused Ga+ ion beam [47,48].

In order to investigate the effect of segregation of Zn and Ag to precipitate-matrix interfaces on twinning, grains with orientations favoring the activation of this deformation mechanism were selected in the three homogenized and aged alloys. Grain selection was carried out using the 3D orientation information from EBSD measurements. Single crystalline micropillars with 5 × 5 $\mu m^2$ cross-section and with an aspect ratio of 2 were milled using a focused Ga+ ion beam at the interior of the selected grains in the three alloys under investigation in both the homogenized and aged conditions. An accelerating voltage of 30 kV and a beam current ranging from 9.3 nA to 2.5 nA was used first for coarse milling under a tilt angle of 52°, and then the beam current was reduced to 80 pA to polish the side surfaces of the milled micropillars and to eliminate the taper under a tilt angle of 53°.

Room temperature (RT) micropillar compression was conducted on a Hysitron TI950 TriboindenterTM using a flat diamond punch with a diameter of 15 mm. The tests were performed using a strain rate of 1 × $10^{-3}$ $s^{-1}$ up to strains of 5 and 15% under a displacement-controlled mode. At least three samples were compressed in each condition to

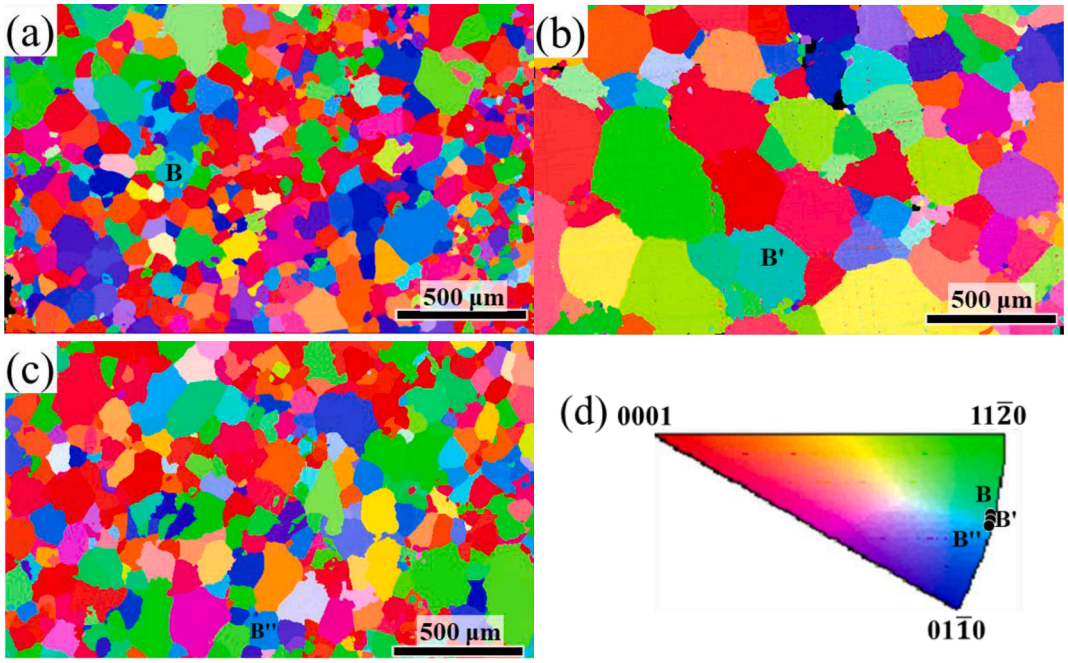


**Fig. 2.** EBSD inverse pole figure maps in the direction normal to the surface of the aged polycrystalline Mg alloys: (a) Mg-8 wt% Al, (b) Mg-8 wt% Al-1 wt% Zn, (c) Mg-8 wt% Al-1 wt% Ag. The grains selected for micropillar compression, named, respectively, B, B′, and B″, are highlighted in bold letters in each map. (d) Inverse pole figure showing the orientation of the normal to the surface (parallel to the compression axis in the corresponding micropillar compression tests) in the selected grains, as well as the color coding for the EBSD inverse pole figure maps.

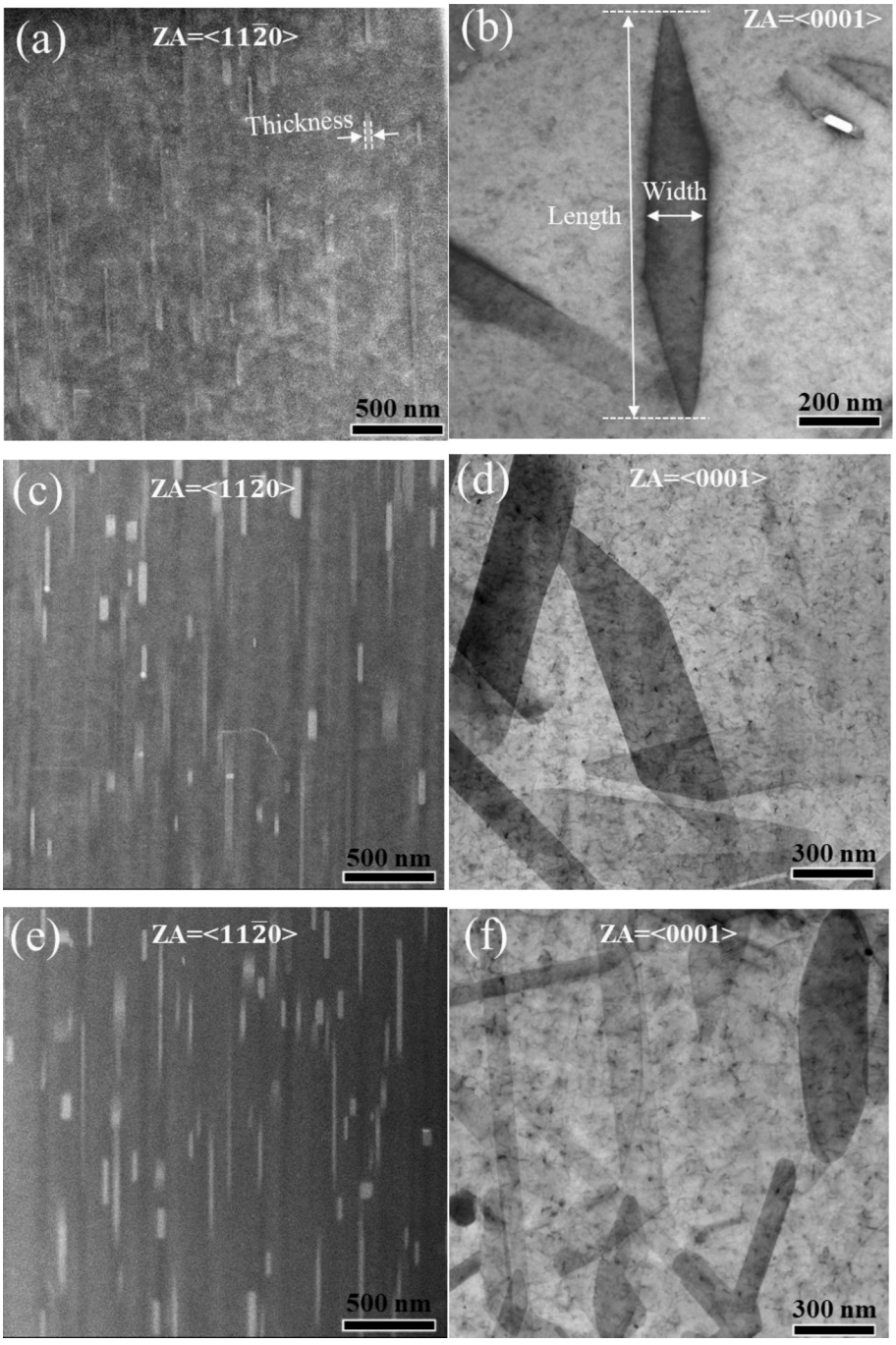


**Fig. 3.** BF STEM (a, c and e) and BF-TEM (b, d and f) images of the aged Mg-Al (a and b), Mg-Al-Zn (c and d) and Mg-Al-Ag (e and f) alloys. Viewing was carried out along the $<11\bar{2}0>_{\alpha}$ (a, c and e) and $<0001>_{\alpha}$ (b, d and f) zone axes. The length, width, and thickness dimensions are highlighted graphically in (a) and (b).

ensure reproducibility. The load-displacement data were treated using the Sneddon-correction, and then they were converted to engineering stress-strain data considering the geometric dimensions of the micropillars. The active modes of deformation during micropillar compression of the homogenized and aged alloys were first investigated by SEM examination of the micropillar surfaces and then they were further confirmed by BF-TEM examination of lamellae extracted parallel to a longitudinal cross-section of the compressed micropillars.

## 3. Results

### *3.1. Microstructure of the homogenized and aged Mg-Al, Mg-Al-Zn, and Mg-Al-Ag alloys*

Fig. 1 illustrates the microstructure of the solid solution Mg-Al (Fig. 1a), the Mg-Al-Zn (Fig. 1b), and the Mg-Al-Ag (Fig. 1c) alloys in the homogenized condition. The equiaxed grain morphology of these three materials is illustrated via the corresponding EBSD inverse pole figure maps in the direction normal to the surface of the samples. The average grain sizes are, respectively, 110, 140, and 101 mm. In order to investigate the effect of Zn and Ag solutes on the active deformation mechanisms and on the mechanical behavior of the homogenized alloys,

**Table 2**
Dimensions and number density of precipitates in the aged alloys.

| Alloy | Length (nm) | Width (nm) | Thickness (nm) | Number density ($mm^{-2}$) |
|---|---|---|---|---|
| Mg-Al | 1368 ± 142 | 171 ± 37 | 33 ± 11 | 0.93 |
| Mg-Al-Zn | 1587 ± 134 | 212 ± 64 | 48 ± 16 | 0.82 |
| Mg-Al-Ag | 1503 ± 325 | 152 ± 40 | 37 ± 10 | 0.99 |

single crystalline micropillars with 5 × 5 $\mu m^2$ square cross-section were milled at the center of selected grains in the three alloys under investigation. The grains that were chosen for the micromechanical study are labelled, respectively, as A, A′, and A″, in Fig. 1. It can be appreciated that their size is sufficiently large to ensure a negligible influence of the grain boundaries on the micromechanical tests. The directions perpendicular to the surface in the three selected grains, which are parallel to the compression axis during micromechanical testing, are plotted in the inverse pole figure of Fig. 1d. In all cases the compression axes are perpendicular to the ⟨0001⟩ direction and they are similarly oriented in the three alloys under investigation. Table 1 summarizes the Euler angles ($\varphi_1$, $\phi$, $\varphi_2$) and the Schmid factors (SFs) corresponding to basal ($SF_{basal}$), prismatic ($SF_{prism}$), and {11–22} pyramidal ($SF_{pyr}$) slip systems, as well as to tensile twinning ($SF_{twin}$) of the selected grains in the homogenized alloys. In all cases, the SF corresponding to basal slip, the softest deformation mechanism, is very low ($SF_{basal} \leq 0.03$) and thus it is not expected that this mechanism will become active in the Mg matrix during micropillar compression. On the other hand, the SFs corresponding to tensile twinning and to non-basal slip systems are very high ($SF_{twin} \geq 0.44$, $SF_{prism} \geq 0.49$, $SF_{pyr} \geq 0.42$). Since the critical resolved shear stress of twinning ($CRSS_{twin}$) is significantly lower than that of prismatic and pyramidal systems [49,50], it is expected that twinning will become active upon yielding.

Fig. 2 illustrates the microstructure of the Mg-Al (Fig. 2a), the Mg-Al-Zn (Fig. 2b), and the Mg-Al-Ag (Fig. 2c) alloys in the aged condition by means of several EBSD inverse pole figure maps in the direction normal to the surface of the samples. The average grain sizes are, respectively, 99, 183, and 139 mm. Fig. 3 contains several bright field STEM (Fig. 3a, c,e) and TEM (Fig. 3b,d,f) micrographs illustrating the homogeneous distribution of $Mg_{17}Al_{12}$ basal plates resulting from the aging treatment in the Mg-Al (Fig. 3a,b), Mg-Al-Zn (Fgs. 3c,d) and Mg-Al-Ag (Fig. 3e,f) alloys. $Mg_{17}Al_{12}$ particles appear brighter than the matrix in the STEM micrographs because of the higher atomic mass of Al in comparison with Mg. The corresponding average particle dimensions (length, width, and thickness, see their definition in Fig. 3), measured from several TEM micrographs, as well as the precipitate number density, are summarized in Table 2. It can be seen in this table that the b-precipitate distributions

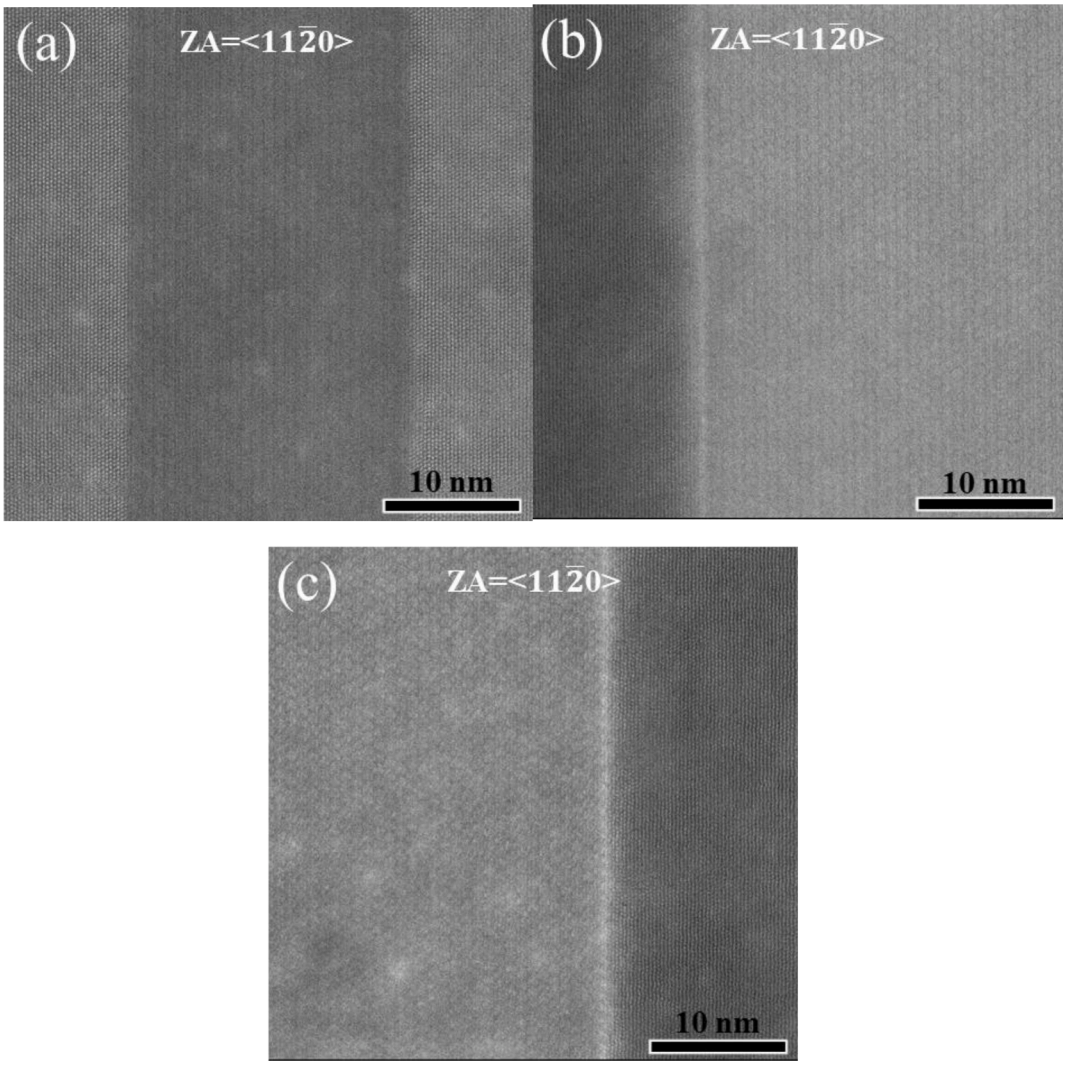


**Fig. 4.** High resolution bright field STEM images of precipitate-matrix interfaces in the aged (a) Mg-Al, (b) Mg-Al-Zn, and (c) Mg-Al-Ag alloys. Viewing was performed along the $<11\bar{2}0>_\alpha$ zone axis.

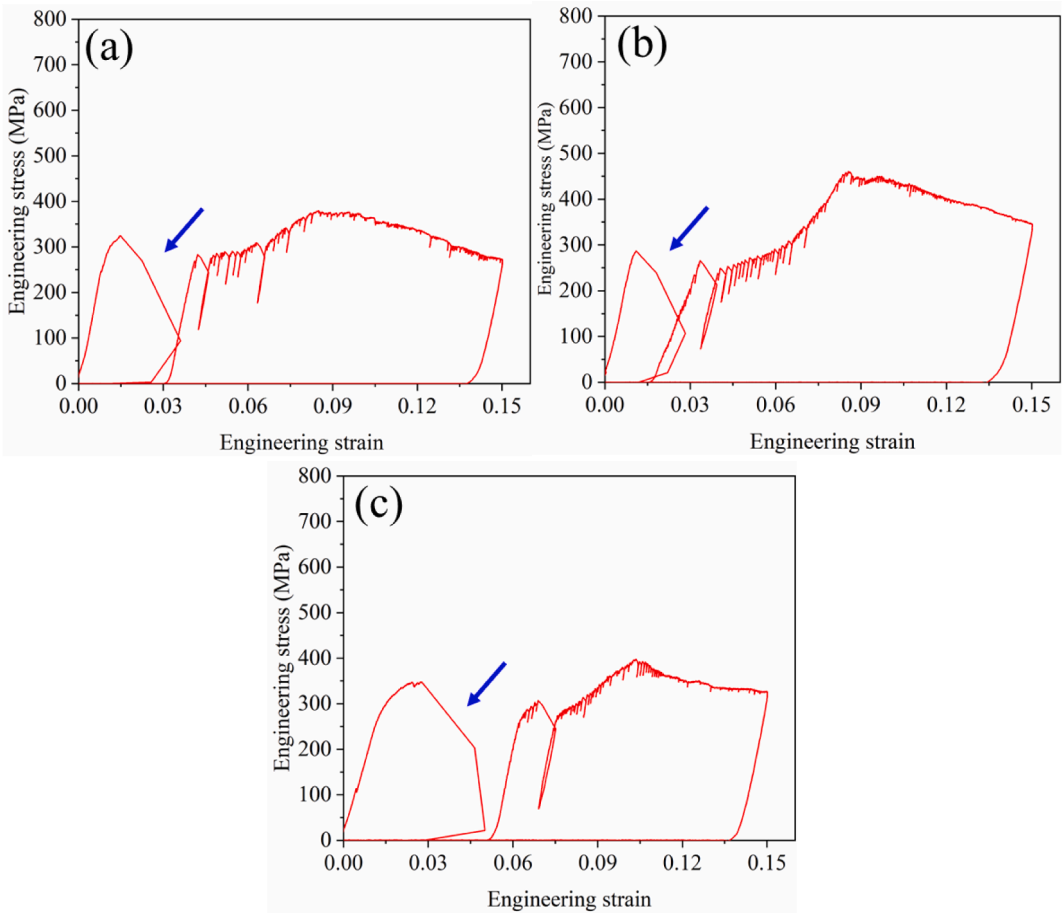


**Fig. 5.** Representative room temperature engineering stress-engineering strain curves obtained from micropillar compression tests performed within selected grains in the homogenized alloys. (a) Mg-Al, (b) Mg-Al-Zn, and (c) Mg-Al-Ag. Blue arrows indicate the strain bursts that are characteristic of the nucleation and propagation of twinning at the early deformation stages.

are very similar in the three alloys investigated. The rather large size of the $Mg_{17}Al_{12}$ basal plates has been put forward as the cause of the poor capability of these particles to strengthen basal slip in Mg-Al alloys [46]. A small fraction of Ag-containing particles, of about 100 nm in size, is also present in the ternary Mg-Al-Ag alloy. As will be reasoned later, the presence of these particles has a minor effect on twin suppression.

Fig. 4 provides a high magnification view of the particle-matrix interfaces in the Mg-Al (Fig. 4a), Mg-Al-Zn (Fig. 4b), and Mg-Al-Ag (Fig. 4c) systems by means of high resolution STEM micrographs captured along the $<11\text{–}20>_{\alpha}$ zone axis. This figure reveals that, while the particle-matrix interface in the binary alloy (Fig. 4a) is clean, several atomic layers of Zn or Ag atoms are clearly present at the particle-matrix interfaces in the ternary alloys (Fig. 4b and 4c, respectively). Segregated layers are apparent along the entire perimeter of the precipitates as brighter regions in the STEM micrographs due to the larger atomic mass of Zn and Ag in comparison to that of Al and Mg.

In order to investigate the effect of Zn and Ag segregation on the active deformation mechanisms and on the mechanical behavior of the aged alloys, micropillars with 5 × 5 $\mu m^2$ square cross-section were milled at the center of selected grains in the three aged alloys under investigation. The grains that were chosen for the micromechanical study are labelled, respectively, as B, B′, and B″, in Fig. 2. Special care was given to select sufficiently large grains in order to avoid spurious grain boundary effects and to limit the potential introduction of grain boundaries under the sample surface. The normal directions in the three selected grains, which are parallel to the compression axis during micromechanical testing, are plotted in the inverse pole figure of Fig. 2d. They are, in all cases, perpendicular to the ⟨0001⟩ direction and have a similar orientation to those of the selected grains in the homogenized alloys (Fig. 1). Table 1 summarizes the Euler angles ($\varphi_1$, $\phi$, $\varphi_2$) and the values of $SF_{basal}$, $SF_{prism}$, $SF_{pyr}$, and $SF_{twin}$ in the selected grains of the aged alloys. It can be seen that $SF_{basal} \leq 0.05$ and thus it is not expected that this mechanism will become active during micropillar compression. On the other hand, the Schmid factors corresponding to tensile twinning and to non-basal slip systems also have very high values ($SF_{twin} \geq 0.46$, $SF_{prism} \geq 0.49$, $SF_{pyr} \geq 0.43$) in the grains selected in the aged alloys. Again, since $CRSS_{twin} < CRSS_{prism,pyr}$, it is expected that twinning will be favored upon yielding.

### 3.2. *Twinning and slip activity in the homogenized Mg-Al, Mg-Al-Zn, and Mg-Al-Ag alloys*

Fig. 5 depicts representative RT compressive engineering stress-engineering strain curves corresponding to the Mg-Al (Fig. 5a), Mg-Al-Zn (Fig. 5b), and Mg-Al-Ag (Fig. 5c) alloys in the homogenized condition. In all cases the initial linear elastic response is followed by a pronounced strain burst and an unloading step, which are indicative of the nucleation and propagation of a twin at the onset of deformation in a single crystalline micropillar [48,49]. The moderate strain reversal associated with the unloading step is due to the momentary loss of contact between the punch and micropillar due to fast twin propagation. Strain hardening then takes place up to an applied strain of 9–10%. We note that there is a minor degree of plasticity before twinning in the ternary Mg-Al-Ag alloy (Fig. 5c), while this effect is much less evident in the other two materials (Fig. 5a,b). As can be seen in Fig. 5, the twin nucleation stress is higher in the ternary Mg-Al-Ag alloy than in the

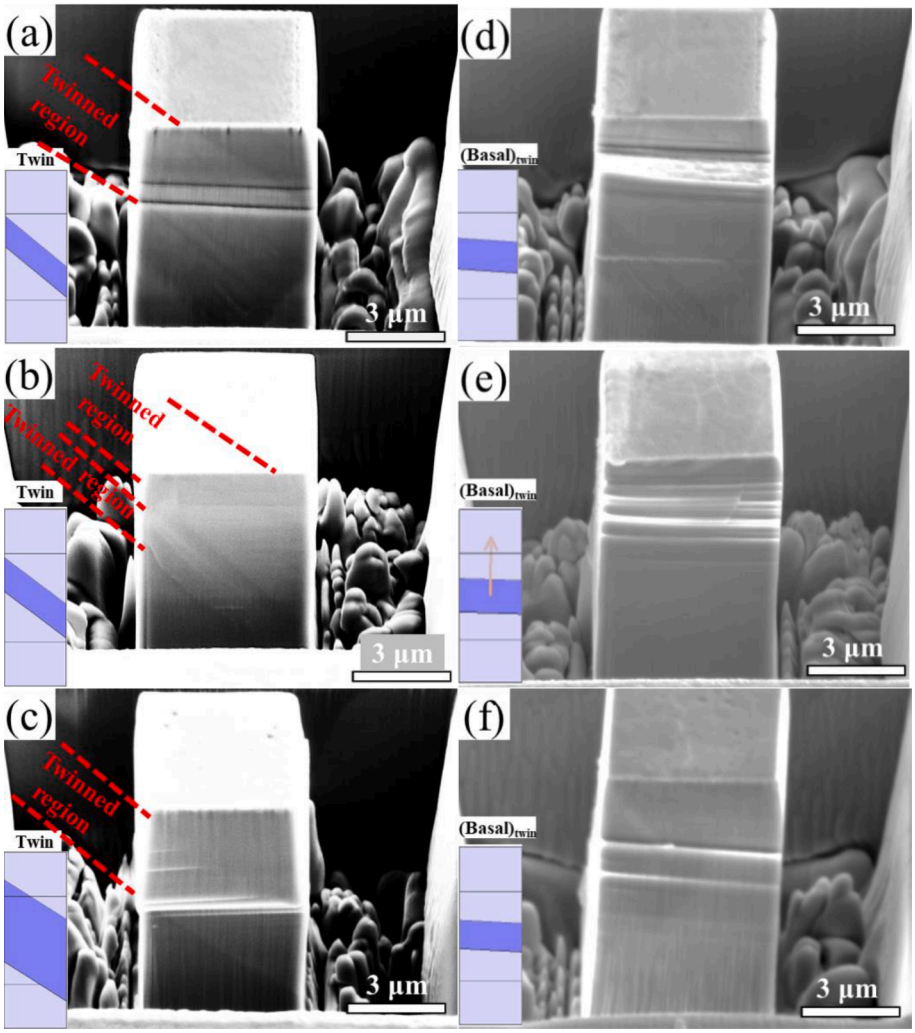


**Fig. 6.** SEM micrographs illustrating the surface of the micropillars milled in the three homogenized alloys following room temperature compression to different strains: (a) Mg-Al alloy, 5% strain; (b) Mg-Al-Zn alloy, 5% strain; (c) Mg-Al-Ag alloy, 5% strain; (d) Mg-Al alloy, 15% strain; (e) Mg-Al-Zn alloy, 15% strain; (f) Mg-Al-Ag alloy, 15% strain. The red dotted lines highlight the boundaries of the twinned regions. The schematics included as insets next to each micrograph illustrate, in blue, the trace of the corresponding deformation mechanisms.

other two investigated materials. However, we must note that identifying when twins first form as embryos is challenging to detect. The embryos are nanoscale in size [51–53]. The amount of strain accommodated by a twin scales with its volume. When twins first form (1) they are hard to detect and (2) they are too small to accommodate strain at a level that would be detectable in a macroscopic stress-strain curve.

Fig. 6a–c illustrate, respectively, the surfaces of the micropillars milled in the homogenized Mg-Al, Mg-Al-Zn, and Mg-Al-Ag alloys after a compression strain of 5%. Twinned regions are highlighted in this figure using red dotted lines. As expected, a significant portion of the micropillars has undergone twinning at a strain of 5%. Basal slip traces are also visible inside the twins, as has been reported earlier in both experimental [54,55] and computational studies [56,57]. Fig. 7, which includes several bright field TEM images of cross-sections of the micropillars parallel to the compression axis, confirms the presence of large twinned regions and of basal slip inside the twins in the three homogenized alloys after a strain of 5%. The twin area fraction, measured from the TEM micrographs in Fig. 7, amounts to 75% in the Mg-Al alloy, to 61% in Mg-Al-Zn alloy, and to 40% in the Mg-Al-Ag alloy. As these twin fractions were measured from only one TEM lamella each, the exact numbers must be taken with caution. Since twin nucleation is known to take place at the micropillar surfaces, small changes in the defect density of such surfaces might lead to different twin nucleation stresses and, thus, to different degrees of twin propagation. Nevertheless, the high twin area fractions reported above are consistent with the easiness of twin propagation and growth in the three homogenized alloys. Fig. 6d–f illustrate, respectively, the surfaces of the micropillars milled in the homogenized Mg-Al, Mg-Al-Zn, and Mg-Al-Ag alloys after a compression strain of 15%. Traces of basal slip inside the twins become more numerous and more distinct at this higher strain. The activation of basal slip inside the twinned regions is responsible for the strain hardening observed up to strains of 9–10%, in agreement with earlier studies [54].

Table 3 summarizes the yield strength (YS) and the ultimate tensile strength (UTS) corresponding to the RT compression tests of the three homogenized alloys investigated (Fig. 5). The YS was measured as the strain at which the initial strain burst takes place. The $CRSS_{twin}$ was calculated from the YS by multiplying for the corresponding $SF_{twin}$. It can be seen that the addition of Zn and Ag does not lead to any major change in the YS, UTS, and $CRSS_{twin}$ values.

In summary, our results suggest that ternary alloying with Zn and Ag in solid solution does not prevent the formation of thick twin lamellae spanning the entire width of the micropillars, i.e., that these solute additions do not hinder severely twin propagation and growth in Mg-Al alloys.

### 3.3. *Twinning and slip activity in the aged Mg-Al, Mg-Al-Zn, and Mg-Al-Ag alloys*

Fig. 8 depicts representative RT compressive engineering stress-engineering strain curves corresponding to the Mg-Al (Fig. 8a), Mg-Al-Zn (Fig. 8b), and Mg-Al-Ag (Fig. 8c) alloys in the aged condition. In

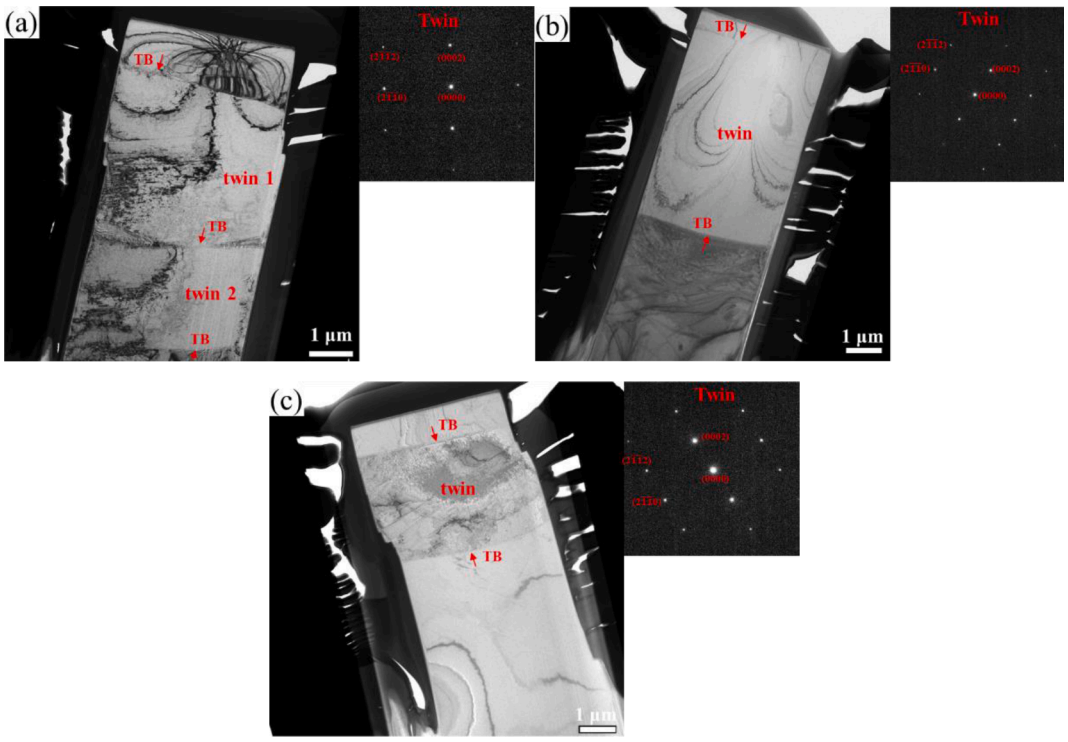


**Fig. 7.** Bright field TEM images illustrating the presence of large twinned regions in the micropillars milled in the homogenized alloys and compressed up to a strain of 5%: (a) Mg-Al, (b) Mg-Al-Zn, (c) Mg-Al-Ag. The red arrows point toward the twin boundaries (TB). Selected area diffraction (SAD) patterns are included as insets. Several spots have been indexed to facilitate a better understanding of the orientation of the lattice within the twinned regions. The zone axis is ⟨10–10⟩.

**Table 3**
Average room temperature YS, $CRSS_{twin}$, and UTS measured from the micro-mechanical tests performed in the homogenized and aged alloys under investigation.

| Alloy | Condition | Average YS (MPa) | Average $CRSS_{twin}$ (MPa) | Average UTS (MPa) |
|---|---|---|---|---|
| Mg-Al | Homogenized | 254 ± 45 | 117 ± 21 | 357 ± 31 |
| | Aged | 204 ± 37 | 95 ± 17 | 711 ± 13 |
| Mg-Al-Zn | Homogenized | 248 ± 38 | 117 ± 18 | 448 ± 18 |
| | Aged | 259 ± 15 | | 693 ± 20 |
| Mg-Al-Ag | Homogenized | 257 ± 48 | 113 ± 21 | 345 ± 74 |
| | Aged | 272 ± 23 | | 702 ± 27 |

the binary alloy the initial linear elastic response is followed by several relatively large strain bursts (albeit smaller than those observed in the homogenized alloy) and abrupt unloading steps, which are consistent with the nucleation, propagation and growth of several twin lamellae. However, in the ternary systems, only minor stress drops take place, and strain bursts are basically absent, suggesting limited twin propagation and growth. In all systems, pronounced strain hardening takes place at strains larger than approximately 6%.

The effect of aging on twin development during deformation is investigated further by the examination of the surfaces of aged binary and ternary alloy deformed micropillars by SEM (Fig. 9) and of micropillar longitudinal cross-sections by TEM (Fig. 10). Let us first focus on the binary alloy. Fig. 9a illustrates the surface of the aged Mg-Al micropillar milled after RT compression up to a strain of 5%. Twinned regions are highlighted using red dotted lines. A significant portion of the binary Mg-Al micropillar is twinned, and this is consistent with the presence of several strain bursts at the early deformation stages (Fig. 8a). Fig. 10a, which consists of a bright field TEM image of a cross-section of the Mg-Al micropillar parallel to the compression axis, confirms the presence of several thick twin lamellae in the aged binary alloy after a strain of 5%. The corresponding twin area fraction is 66% and the average twin lamella thickness is 1690 ± 620 nm. Our results, therefore, reveal, that the presence of the $Mg_{17}Al_{12}$ plates in the aged binary alloy *does not* severely prevent twin propagation and growth. Fig. 9d illustrates the surface of the aged Mg-Al micropillar after RT compression up to a strain of 15%. Traces corresponding to the activation of basal and pyramidal slip inside the twinned regions are clearly apparent. Fig. 11 confirms the presence of pyramidal dislocations inside a twin lamella in the Mg-Al alloy micropillar compressed at RT up to a strain of 7%. The large strain hardening observed at strains larger than about 6% (Fig. 8) is consistent with the presence of basal and non-basal dislocations inside the twins by the $Mg_{17}Al_{12}$ plates, which lay on prismatic planes due to the twin lattice rotation.

Table 3 lists the YS and the UTS of the aged binary alloy. The YS was measured as the strain at which the initial strain burst takes place. The $CRSS_{twin}$ was calculated from the YS by multiplying for the corresponding $SF_{twin}$. Aging appears to soften twinning, in agreement with earlier studies [36,58,59]. However, perhaps the most remarkable effect of aging in the binary alloy is the very large UTS value obtained, close to 700 MPa, which, as stated above, is attributed to particle hardening of basal and pyramidal systems inside the twinned regions.

While in the binary alloy aging does not seem to have a very strong influence on the twin activity, in the ternary alloys it does lead to a significant degree of twin suppression. The surfaces of aged Mg-Al-Zn and Mg-Al-Ag micropillars following RT compression up to strains of 5% are shown in Fig. 9b and c, respectively, by means of SEM secondary electron images. No signs of twinning could be detected in the surfaces of the ternary alloy micropillars. The bright field TEM micrographs of Fig. 10b and c reveal, however, the presence of thin twin lamellae in Mg-Al-Zn and Mg-Al-Ag micropillars, respectively, after a 5% strain. The average twin widths in the Zn-containing and Ag-containing alloys are, respectively, 260 ± 80 nm and 190 ± 90 nm. The corresponding twin area fractions are, respectively, 8% and 4%. It must be noted that all the twin lamellae correspond to the same variant, and that some twin tips are arrested at the micropillar interior, indicating that twin propagation was hindered by the presence of the particles. The above observations

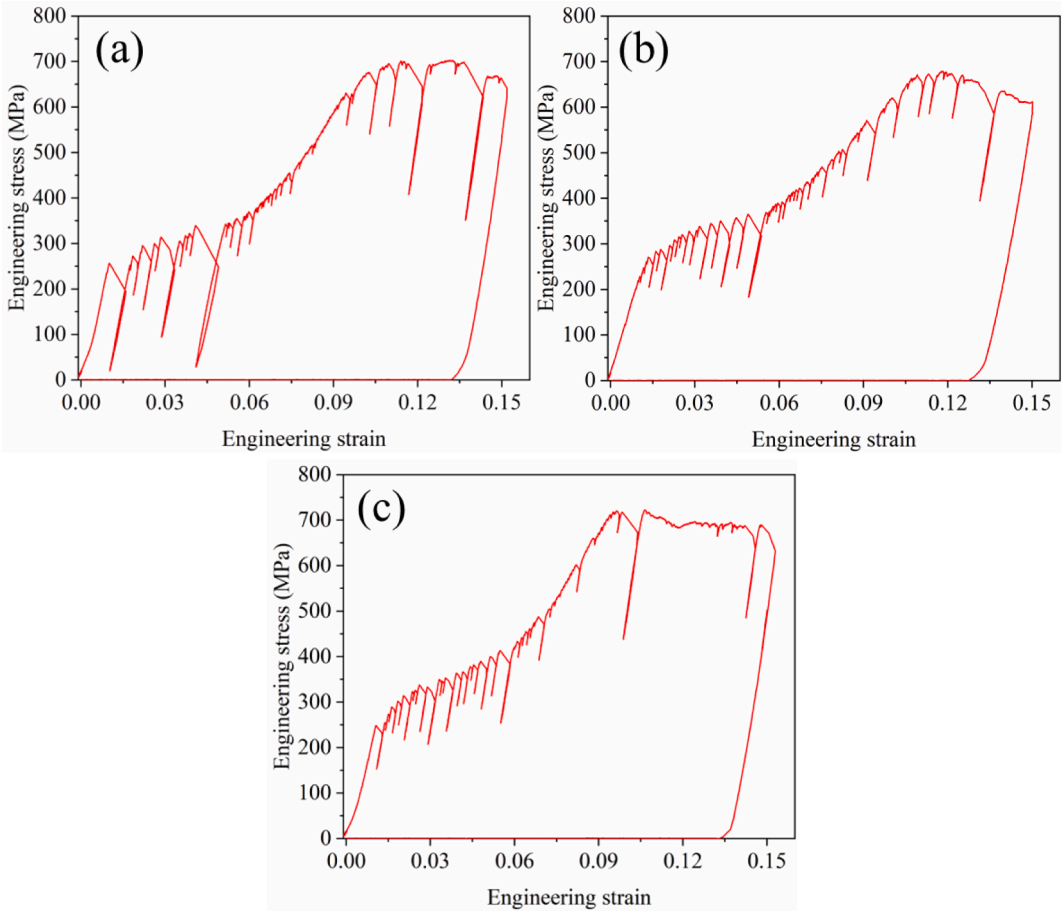


**Fig. 8.** Representative room temperature engineering stress-engineering strain curves obtained from micropillar compression tests performed within selected grains in the aged alloys. (a) Mg-Al, (b) Mg-Al-Zn, and (c) Mg-Al-Ag.

are consistent with the absence of unloading steps and of significant strain bursts in the stress-strain curves at the early deformation stages (Fig. 8b and c). Fig. 9e and f show that, after a strain of 15%, the surfaces of the ternary alloy micropillars are populated with matrix pyramidal slip traces, but no sign of basal slip activation is apparent. The absence of basal slip traces is consistent with the low $SF_{basal}$ in the matrix. TEM was carried out in order to verify whether basal slip inside twins could still have taken place without leading to the development of noticeable surface traces due to the small thickness of the twin lamellae. Fig. 12 illustrates the dislocation activity inside a twinned region in the Mg-Al-Ag alloy after a strain of 7%. It can be seen that, indeed, both basal slip and pyramidal slip are present inside the twin.

Table 3 summarizes the YS and the UTS of the aged ternary alloy micropillars. Since the twinning activity is drastically reduced in these materials, it is not clear whether yielding takes place by the activation of twinning or by the simultaneous activation of twinning and slip, and thus $CRSS_{twin}$ was not calculated from the YS. The high UTS achieved in the ternary alloys, close to 700 MPa, may be attributed to precipitation hardened basal and pyramidal slip inside the twins, as well as to precipitation hardened pyramidal slip in the matrix.

## 4. Discussion

This research shows that, while single variant thick twin lamellae develop during the first stages of deformation in all the homogenized alloys and in the binary aged alloy, in the aged ternary alloys the twin fraction decreases drastically and only narrow twin lamellae, also belonging to the same variant and occasionally arrested at micropillar interiors, are apparent. The observed reduction in the twinning activity cannot be due to the presence of some remnant ternary elements in solid solution [60], as we have shown (Section 3.2) that the latter have only a minor influence on twin propagation and growth. Also, such a pronounced change in the twin activity cannot be attributed to an alteration of the precipitate distribution via ternary alloying as the three materials under investigation have comparable particle sizes and number densities (Table 2). Instead, our work suggests that the segregation of ternary elements (such as Zn and Ag) to the interfaces between the $Mg_{17}Al_{12}$ basal plates and the Mg matrix is the cause of the reduced twinning activity. In the following, this observation is rationalized in light of the existing literature.

### 4.1. Twin re-nucleation at particle-matrix interfaces

Twins are known to nucleate profusely at grain boundaries and at free surfaces [26]. Additionally, in a recent work, Xie et al. [31] observed profuse twin nucleation at particle-matrix interfaces in an aged Mg-9%Al (wt%) alloy. These authors investigated the types of interaction of twins and basal precipitates with the aid precession electron diffraction in compressed aged single crystalline micropillars favorably oriented for tensile twin activation. According to this study, when twin tips are fully arrested by basal precipitates, a phenomenon that occurs statistically more frequently is that the impinging twin thickness ($t_t$) is significantly larger than the precipitate length ($t_p$), that is, equivalently, when $(t_p/t_t) < 1$. For such cases, they conjectured that re-nucleation of a new twin may take place at another location of the precipitate-matrix interface due to the generation of local stress concentrations, as illustrated schematically in Fig. 13. Evidence of blocking of thin twin tips by large basal plates and re-nucleation at precipitate boundaries has also

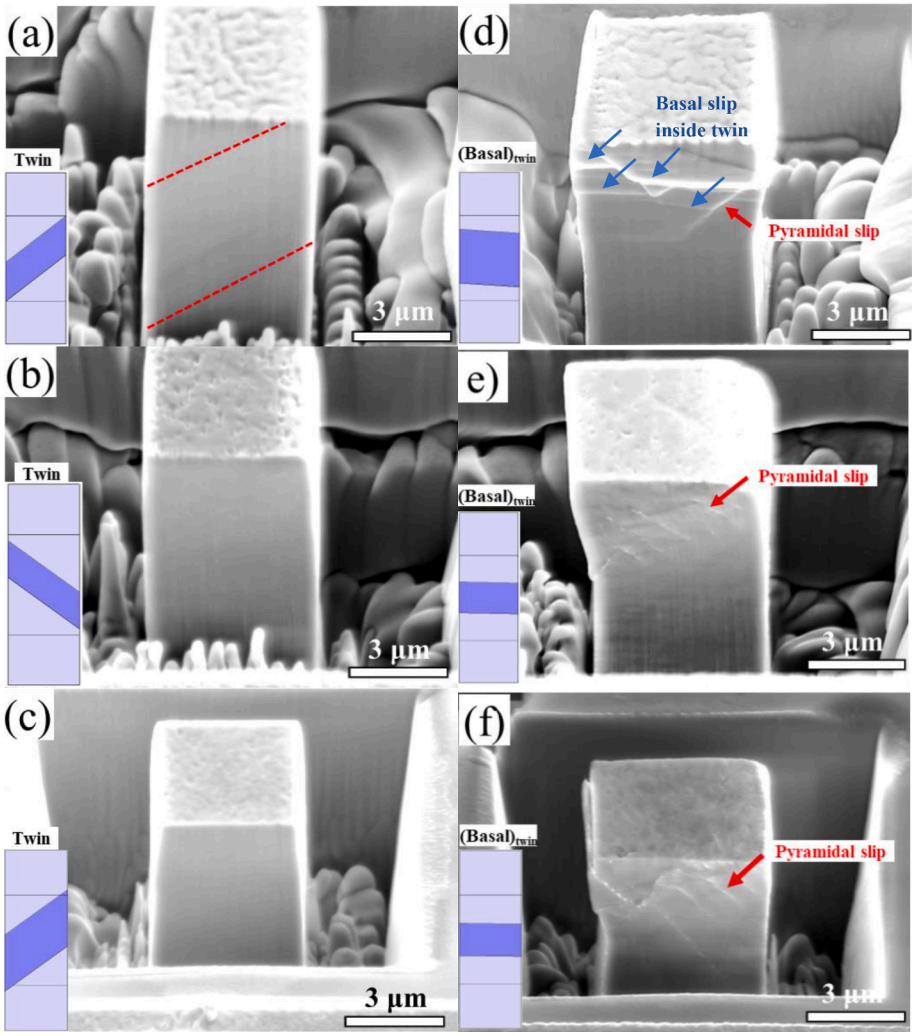


**Fig. 9.** SEM micrographs illustrating the surface of the aged alloy micropillars following room temperature compression to different strains: (a) Mg-Al, 5% strain; (b) Mg-Al-Zn, 5% strain; (c) Mg-Al-Ag, 5% strain; (d) Mg-Al, 15% strain; (e) Mg-Al-Zn, 15% strain; (f) Mg-Al-Ag, 15% strain. The red dotted lines highlight the boundaries of the twinned regions. The schematics included as insets next to each micrograph illustrate, in blue, the trace of the corresponding deformation mechanisms. Red arrows indicate pyramidal slip traces.

been reported in [23,31,39,61]. In the current study, in the Mg-Al, Mg-Al-Zn, and Mg-Al-Ag alloys, the ($t_p/t_t$) ratios amount, respectively, to 0.14, 0.2, 0.4, where $t_t$, is approximately 200 nm, making continued growth via re-nucleation a possible mechanism.

Later, using an elasto-viscoplastic fast-Fourier-transform (EVP-FFT) model, Leu-et al. [62,63] determined that, in particular, the likelihood of re-nucleation at the *opposite* side of the precipitate increases when $t_p/t_t < 1$. They also calculated that the twin resolved shear stress ($RSS_{twin}$) at the opposite side of the precipitate would be higher for both the same variant as the impinging twin, or for the cozone variant. Thus, under these conditions, precipitates have a relatively small shielding capacity and twins would appear to "hop" over the precipitate. After the twin hopped, the stress state changes favoring growth of the impinging twin. In this way, the twin can bypass the precipitate and even grow around it.

In all three alloys studied here, the stress state alone should favor initial twin hopping over precipitates and single variant twins could predominate in the three alloys investigated. This is, indeed, what is observed in the binary alloy (Fig. 10a). In the aged ternary alloys, however, the twins, once pinned by a precipitate, do not continue to grow around it. The difference might be because re-nucleation is not supported at the precipitate/matrix interface, which likely has a reduced interface energy resulting from the presence of segregated atoms.

It was mentioned earlier that a minor fraction of small (approximately 100 nm in size) Ag-containing particles is present in the ternary Mg-Al-Ag alloy. As shown graphically in Fig. 13, and as reported by Xie et al. [31] effective stopping of twin lamellae requires significantly longer precipitates, on the order of the thickness of the impinging twin lamellae, and thus the influence of the Ag-containing particles on the twin activity is expected to be negligible.

### 4.2. *Effect of Zn and Ag segregation on the particle-matrix interface energy*

The interface between the Mg matrix and $Mg_{17}Al_{12}$ plates, recently characterized using HR-TEM by Liu et al. [44], includes a 3.2% misfit strain, as semi-coherent, which is accommodated by misfit dislocations separated by about 25–32$d_{(01\text{–}1\text{–}1)\alpha}$. Several earlier works have described the tendency of Zn and Ag atoms to segregate to precipitate-matrix interfaces in Mg alloys and assume a periodic arrangement. In an aged Mg-9Al-3 Zn (wt%) alloy, Liu et al. [44] reported the segregation of Zn to the semi-coherent interface of basal $Mg_{17}Al_{12}$ precipitates, with the plates parallel to the basal plane. The segregated Zn atoms replace Al atoms in the fully-coherent regions between the misfit dislocations. Miao et al. [45] have observed that Ag segregates to the interface of $Mg_{17}Al_{12}$ plates in an aged Mg-7Al-2Sn-0.7Ag (wt%) alloy, without changing the Burgers orientation relationship with the matrix. Ag atoms reportedly lay along both the long and the short sides of the plates, and Ag layers are located not only at the interface itself, but also several atomic planes away from it. Similarly, Liu et al. [64] have recently reported the segregation of Sn at the Mg matrix atomic layer immediately adjacent to $Mg_3Sn$ particles in an aged Mg-9.8Sn (wt%) alloy. The segregation, ordered arrangement taken, and preservation of the

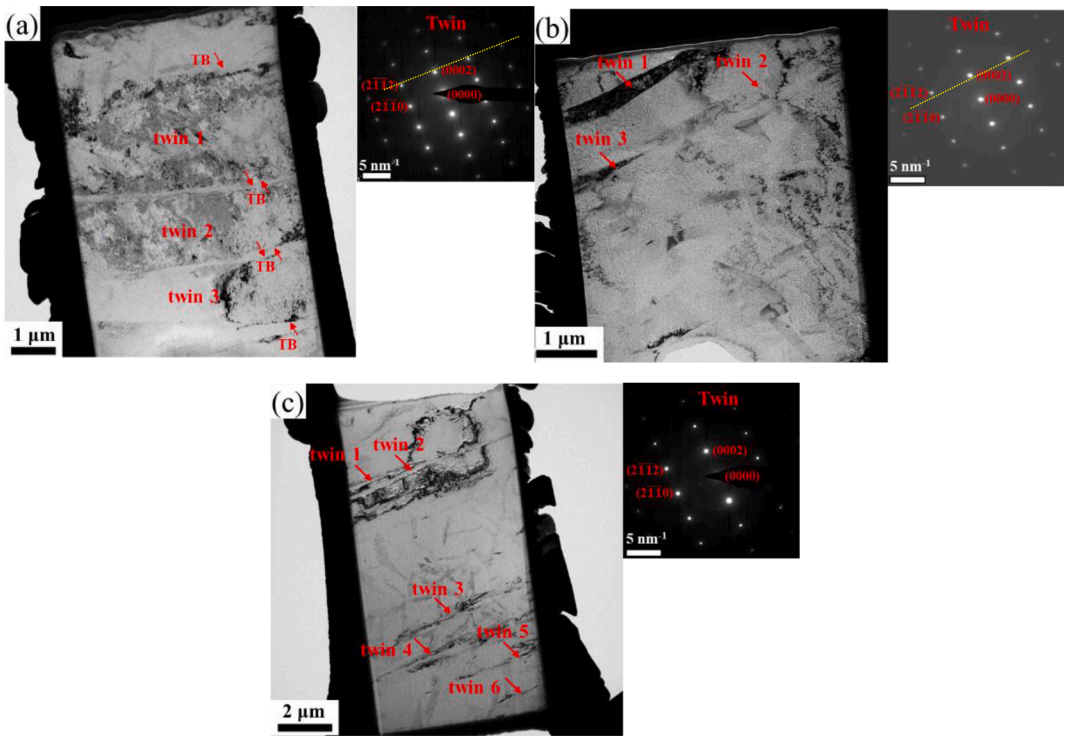


**Fig. 10.** Bright field TEM images illustrating twinned regions in the aged micropillars after a compression strain of 5%: (a) Mg-Al, (b) Mg-Al-Zn, (c) Mg-Al-Ag. The red arrows point toward the twin boundaries (TB). Selected area diffraction (SAD) patterns are included as insets. The yellow dotted lines in the selected area diffraction (SAD) patterns indicate the orientation of the basal plane within twinned regions. Several spots have been indexed to facilitate a better understanding of the orientation of the lattice within the twinned regions. The zone axis is $<10{-}10>_{\alpha}$.

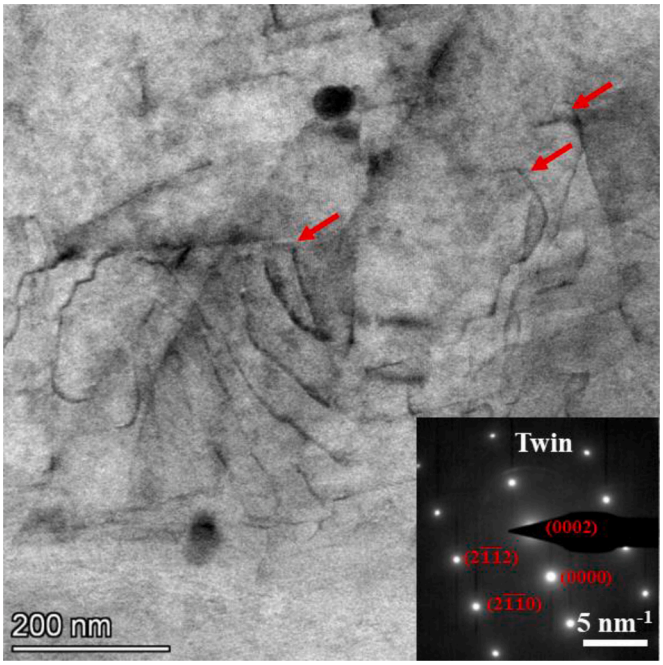


**Fig. 11.** Pyramidal dislocations (red arrows) imaged inside a twinned region in the aged Mg-Al binary alloy micropillar after a compression strain of 7%. Imaging was performed along $a$ $<1 - 100>_{\alpha}$ zone axis under bright field conditions.

semi-coherent interface would suggest that segregation decreases the particle-matrix interfacial energy from that for the semi-coherent interface in the MgAl alloy. In support, first principle calculations have indicated that interphase boundary segregation of Zn, Ag, and Sn in the above Mg alloys is energetically favored [44,45,64].

### 4.3. *Effect of precipitate-matrix interface energy on twin re-nucleation*

Recent studies in Mg have shown that the stabilization of a twin nucleus takes place broadly in two steps, first by the formation of nanoscale twin embryos via pure shuffling followed by their coalescence [52,53]. Twin nucleation is preferable at defects, such as surfaces, cracks, and rough grain and twin boundaries, which are usually defective, and less so at coherent boundaries or in a perfect crystal [65,66]. In particular, atomistic simulations [67] have shown that boundaries containing arrays of grain boundary defects constitute favorable sites for twin nucleation. Similarly, twin nucleation at particle-matrix interfaces should also be sensitive to the energy of these interphase boundaries which, as described above, decreases as a result of ternary alloy segregation. We therefore rationalize that, in the aged ternary alloys of the current study, twin nucleation at the $Mg_{17}Al_{12}$–Mg interfaces is less likely than in the aged binary alloy because the segregation of Zn and Ag decreases the interphase boundary energy. Ultimately, the presence of a smaller number of favorable twin nucleation sites in the ternary alloys would contribute to the drastic reduction in the twin activity observed.

## 5. Conclusions

This work aims to investigate the influence of solute segregation at particle-matrix interfaces on the twin activity of aged Mg-Al alloys. The following conclusions can be drawn from the present study:

(1) In the homogenized condition, ternary alloying with Zn and Ag in solid solution does not hinder severely twin propagation and growth and it does not impede the formation of thick twin lamellae during the early deformation stages. The area fraction of twinning ranges from 40 to 75% in the homogenized alloys.

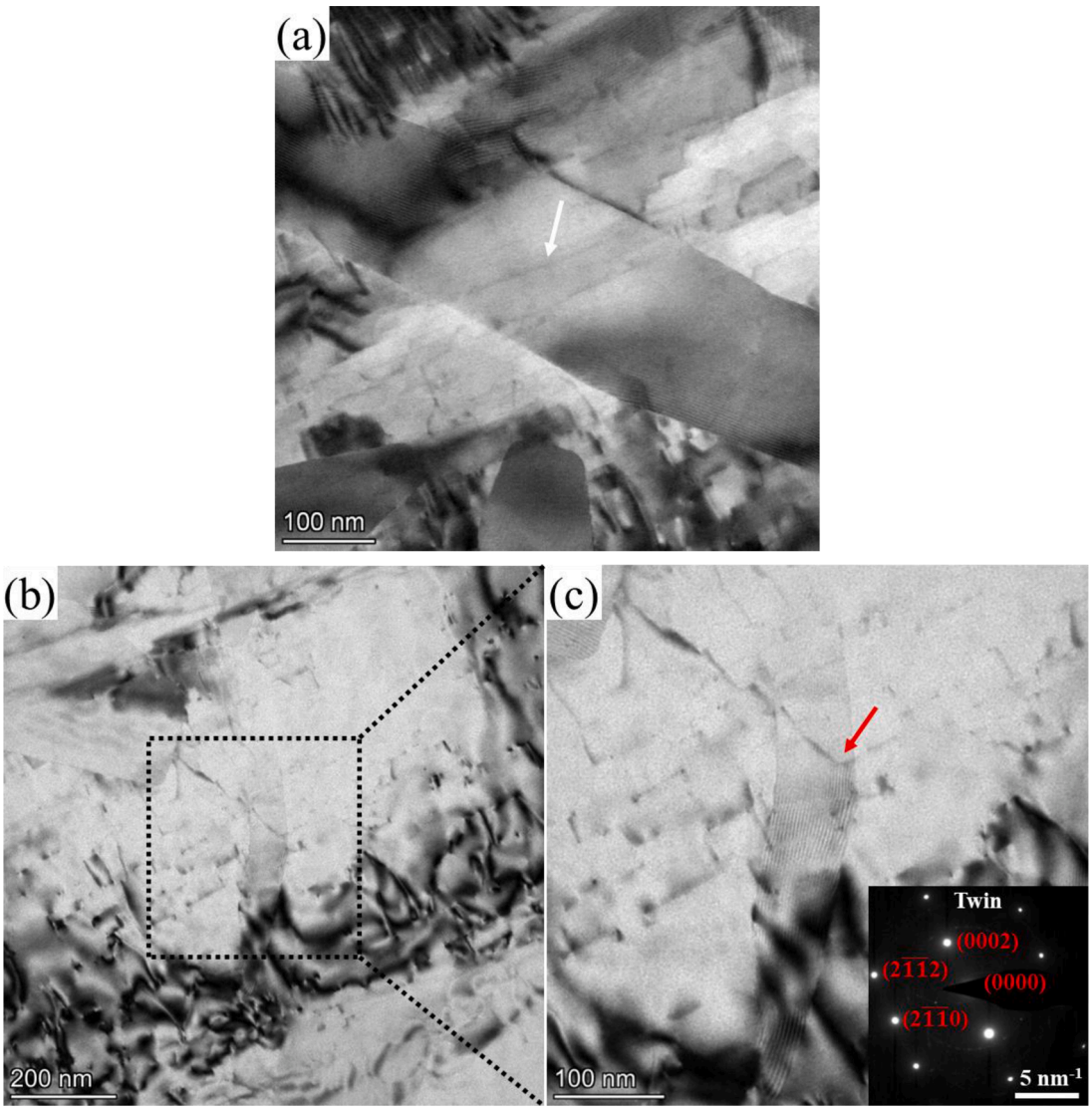


**Fig. 12.** Basal (a, $<11-20>_\alpha$ zone axis, white arrow) and pyramidal (b,c, $<1-100>_\alpha$ zone axis, red arrow) dislocations imaged under bright field conditions inside a twin lamella in an aged Mg-Al-Ag ternary alloy micropillar that was compressed to a strain of 7%.

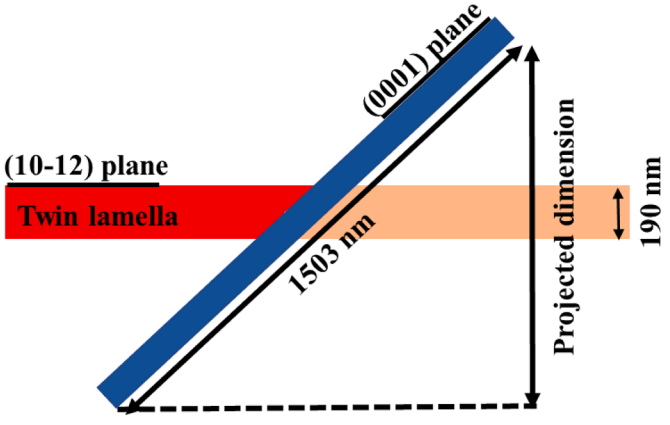


**Fig. 13.** Schematic illustrating a thin twin (red) blocked by a comparatively larger basal plate precipitate (blue), and re-nucleation of another twin (orange) at the opposite side of the particle. The twin and precipitate dimensions correspond to the Mg-Al-Ag alloy. A similar mechanism would apply for the Mg-Al-Zn alloy.

$CRSS_{twin}$ remains basically unchanged by the ternary addition of Zn and Al.

(2) Aging led to comparable precipitate distributions in the binary and ternary alloys in terms of precipitate dimensions and number density. However, while in the binary alloys particle-matrix interfaces are "clean" (i.e., segregation-free), in the ternary alloys Zn and Ag solutes segregate profusely at precipitate-matrix interfaces.

(3) In the aged binary alloy precipitation of basal $Mg_{12}Al_{17}$ plates does not hinder severely twin propagation and growth. The area fraction of twinning remains high and similar to that of the homogenized counterpart. Single variant, thick twin lamellae develop during the early deformation stages. This is consistent with twin re-nucleation at precipitate interfaces opposite to those of the incoming twins, in agreement with earlier predictions of EVP-FFT models.

(4) In the aged ternary alloys the twin activity is considerably reduced. Narrow twin lamellae belonging to a single variant, and occasionally arrested at the interior of the micropillars, develop during the early deformation stages. The twin fraction decreases drastically to values comprised between 4 and 8%. We propose that the reduction of the energy of particle-matrix interfaces due

to the segregation of Zn and Ag hinders re-nucleation at such interfaces, thus suppressing twin propagation.

(5) It is known that twin activity is influenced by the precipitate volume fraction, size, geometry and spatial distribution. This work suggests that segregation at particle-matrix interfaces must also be considered an important microstructural feature influencing twinning in Mg alloys.

## Declaration of Competing Interest

The authors declare that they have no known competing financial interests or personal relationships that could have appeared to influence the work reported in this paper.

## Acknowledgments

The research leading to these results has received funding from the Spanish Ministry of Science, Innovation and Universities under project PID2019–111285RB-I00. I.J.B. gratefully acknowledges support by the National Science Foundation under Grant Number 2051390.

## References

[1] H. Monteiro, R. Alonso, M. Gonçalves, M. Iten, N.S. Caetano, Life cycle energy of vehicles on lightweighting and alternative powertrain strategies—a review, Energy Rep. 8 (2022) 241, 24.
[2] G.M. Lewis, C.A. Buchanan, K.D. Jhaveri, J.L. Sullivan, J.C. Kelly, S. Das, A.I. Taub, G.A. Keoleian, Green principles for vehicle lightweighting, Environ. Sci. Technol. 53 (8) (2019) 4063–4077.
[3] M.T. Pérez-Prado, C.M. Cepeda-Jiménez, Materials science: strength ceiling smashed for light metals, Nature 528 (2015) 486–487.
[4] D. Raabe, C.C. Tasan, E.A. Olivetti, Strategies for improving the sustainability of structural metals, Nature 575 (2019) 64–74.
[5] T.M. Pollock, Weight loss with magnesium alloys, Science 328 (2010) 986–987.
[6] M. Esmaily, J.E. Svensson, S. Fajardo, N. Birbilis, G.S. Frankel, S. Virtanen, R. Arrabal, S. Thomas, L.G. Johansson, Fundamentals and advances in magnesium alloy corrosion, Prog. Mater. Sci. 89 (2017) 92–193.
[7] by C. Bettles, M.R. Barnett, Advances in Wrought Magnesium Alloys, Woodhead publishing, Cambridge, 2012. by.
[8] M.O. Pekguleryuz, K.U. Kainer, A.A. Kaya, Fundamentals of Magnesium Alloy Metallurgy, Woodhead publishing, Cambridge, 2013.
[9] M.T. Pérez-Prado, J. Bohlen, S. Yi, D. Letzig, T. Al-Samman, J. Robson, M. Barnett, W.J. Poole, C.L. Mendis, S. Agnew, N. Stanford, Emerging hot topics and research questions in wrought magnesium alloy development, JOM 72 (2020) 2561–2567.
[10] C.M. Cepeda-Jiménez, M.T. Pérez Prado, Microplasticity-based rationalization of the room temperature yield asymmetry in conventional polycrystalline Mg alloys, Acta Mater. 108 (2016) 304–316.
[11] J. Robson, Anisotropy and asymmetry of yield in magnesium alloys at room temperature, Metall. Mater. Trans. A 45 (2014) 5226–5235.
[12] E.A. Ball, P.B. Prangnell, Tensile-compressive yield asymmetries in high strength wrought magnesium alloys, Scr. Metall. Mater. 31 (1994) 111–116.
[13] M. Arul Kumar, B. Clausen, L. Capolungo, R.J. McCabe, C.N. Tomé, Deformation twinning and grain partitioning in a hexagonal close-packed magnesium alloy, Nat. Commun. 9 (2018) 4761–4769.
[14] A.E. Davis, J.D. Robson, M. Turski, Reducing yield asymmetry and anisotropy in wrought magnesium alloys – a comparative study, Mater. Sci. Eng. A 744 (2019) 525–537.
[15] J. Bohlen, M.R. Nürnberg, J.W. Senn, D. Letzig, S.R. Agnew, The texture and anisotropy of magnesium–zinc–rare earth alloy sheets, Acta Mater. 55 (2007) 2101–2112.
[16] R. Mahjoub, N. Stanford, The electronic origins of the “rare earth” texture effect in magnesium alloys, Sci. Rep. 11 (2021) 14159.
[17] N. Stanford, Micro-alloying Mg with Y, Ce, Gd and La for texture modifcation—a comparative study, Mater. Sci. Eng. A 527 (2010) 2669–2677.
[18] Y. Chino, M. Kado, M. Mabuchi, Enhancement of tensile ductility and stretch formability of magnesium by addition of 0.2 wt.% (0.035 at.%) Ce, Mater. Sci. Eng. A 494 (2008) 343–349.
[19] A. Javaid, F. Czerwinski, Progress in twin roll casting of magnesium alloys: a review, J. Mag. Alloys 9 (2021) 362–391.
[20] N. Stanford, R.K.W. Marceau, M.R. Barnett, The effect of high yttrium solute concentration on the twinning behaviour of magnesium alloys, Acta Mater. 82 (2015) 447–456.
[21] C. Cepeda-Jiménez, J.M. Molina-Aldareguia, M.T. Pérez Prado, Origin of the twinning to slip transition with grain size refinement, with decreasing strain rate and with increasing temperature in magnesium, Acta Mater. 88 (2015) 232–244.
[22] J.D. Robson, N. Stanford, M.R. Barnett, Effect of precipitate shape on slip and twinning in magnesium alloys, Acta Mater. 59 (2011) 1945–1956.
[23] J.D. Robson, M.R. Barnett, The effect of precipitates on twinning in magnesium alloys, Adv. Eng. Mater. (2018), 1800460.
[24] C. Liu, P. Shanthraj, J.D. Robson, M. Diehl, S. Dong, J. Dong, W. Ding, D. Raabe, On the interaction of precipitates and tensile twins in magnesium alloys, Acta Mater. 178 (2019) 146–162.
[25] A. Fernández, A. Jérusalem, I. Gutiérrez-Urrutia, M.T. Pérez Prado, Three dimensional investigation of the grain boundary-twin interactions in a Mg AZ31 alloy by electron backscatter diffraction and continuum modeling, Acta Mater. 61 (2013) 7679–7692.
[26] J.W. Christian, S. Mahajan, Deformation twinning, Prog. Mater. Sci. 39 (1995) 1–157.
[27] J. Jain, W.J. Poole, C.W. Sinclair, M.A. Gharghouri, Reducing the tension-compression asymmetry in magnesium alloys via precipitation, Scr. Mater. 62 (2010) 301–304.
[28] J.D. Robson, N. Stanford, M.R. Barnett, Effect of particles in promoting twin nucleation in a Mg–5 wt% Zn alloy, Scr. Mater. 63 (2010) 823–826.
[29] N. Stanford, M.R. Barnett, Effect of particles on the formation of deformation twins in a magnesium-based alloy, Mater. Sci. Eng. A 516 (2009) 226–234.
[30] P. Hidalgo-Manrique, J.D. Robson, Interaction between precipitate basal plates and tensile twins in magnesium alloys, Metall. Mater. Trans. A 50 (2019) 3855–3867.
[31] K.Y. Xie, D. Zhao, B. Leu, X. Ma, Q. Jiao, J.A. El-Awady, T.P. Weihs, I.J. Beyerlein, M. Arul Kumar, Understanding the interaction of extension twinning and basal-plate precipitates in Mg-9Al using precession electron diffraction, Materialia 15 (2021), 101044.
[32] F. Siska, L. Stratil, J. Cizek, T. Guo, M. Barnett, Numerical analysis of twin-precipitate interactions in magnesium alloys, Acta Mater. 202 (2021) 80–87.
[33] J. Geng, Y.B. Chun, N. Stanford, C.H.J. Davies, J.F. Nie, M.R. Barnett, Processing and properties of Mg–6Gd–1Zn–0.6Zr: part 2. Mechanical properties and particle twin interactions, Mater. Sci. Eng. A 528 (2011) 3659–3665.
[34] S. Si, J. Wu, I.P. Jones, Y.L. Chiu, Influence of precipitates on basal dislocation slip and twinning in AZ91 micro-pillars, Philos. Mag. 100 (2020) 2949–2971.
[35] N. Stanford, J. Geng, Y.B. Chun, C.H.J. Davies, J.F. Nie, M.R. Barnett, Effect of plate-shaped particle distributions on the deformation behaviour of magnesium alloy AZ91 in tension and compression, Acta Mater. 60 (2012) 218–222.
[36] X.Z. Jin, W.C. Xu, D.B. Shan, B. Guo, B. Jin, M.T. Pérez-Prado, A quantitative microplasticity-based approach to rationalize the poor strengthening response of polycrystalline Mg alloys, J. Mag.Alloys (2021) in press.
[37] X.H. Shao, S.J. Zheng, D. Chen, Q.Q. Jin, Z.Z. Peng, X.L. Ma, Deformation twinning induced decomposition of lamellar LPSO structure and its re-precipitation in an Mg-Zn-Y alloy, Sci. Rep. 6 (2016) 30096.
[38] J.B. Clark, Transmission electron microscopy study of age hardening in a Mg-5 wt %Zn alloy, Acta Metall. 13 (1965) 1281–1289.
[39] M.A. Gharghouri, G.C. Weatherly, J.C. Embury, The interaction of twins and precipitates in a Mg-7.7 at.% Al alloy, Philos. Mag. 78 (1998) 1137–1149.
[40] F. Zhang, Y. Ren, Z. Yang, H. Su, Z. Lu, C. Tan, H. Peng, K. Watanabe, B. Li, M. R. Barnett, M. Chen, The interaction of deformation twins with long-period stacking ordered precipitates in a magnesium alloy subjected to shock loading, Acta Mater. 188 (2020) 203–214.
[41] D.F. Shi, C.Y. Wang, C.M. Cepeda-Jiménez, M.T. Pérez-Prado, Atomic scale interaction of basal dislocations and twin boundaries with ultrathin precipitates in magnesium alloys, Acta Mater. 221 (2021), 117442.
[42] Y. Liu, N. Li, S. Shao, M. Gong, J. Wang, R.J. McCabe, Y. Jiang, C.N. Tomé, Characterizing the boundary lateral to the shear direction of deformation twins in magnesium, Nat. Commun. 7 (2016) 11577.
[43] J.F. Nie, Y.M. Zhu, J.Z. Liu, X.Y. Fang, Periodic segregation of solute atoms in fully coherent twin boundaries, Science 340 (2013) 957–960.
[44] C.Q. Liu, H.W. Chen, N.C. Wilson, J.F. Nie, Zn segregation in interface between $Mg_{17}Al_{12}$ precipitate and Mg matrix in Mg–Al–Zn alloys, Scr. Mater. 163 (2019) 91–95.
[45] J. Miao, W. Sun, A.D. Klarner, A.A. Luo, Interphase boundary segregation of silver and enhanced precipitation of $Mg_{17}Al_{12}$ Phase in a Mg-Al-Sn-Ag alloy, Scr. Mater. 154 (2018) 192–196.
[46] J.F. Nie, Precipitation and hardening in magnesium alloys, Metall. Mater. Trans. A 43 (2012) 3891–3939.
[47] C.M. Cepeda-Jiménez, M. Castillo-Rodríguez, M.T. Pérez-Prado, Origin of the low precipitation hardening in magnesium alloys, Acta Mater. 165 (2019) 164–176.
[48] L.A. Giannuzzi, J.L. Drown, S.R. Brown, R.B. Irwin, F.A. Stevie, Applications of the FIB lift-out technique for TEM specimen preparation, Microsc. Res. Tech. 41 (1998) 285–290.
[49] H. Yoshinaga, R. Horiuchi, Deformation mechanisms in magnesium single crystals compressed in the direction parallel to hexagonal axis, Trans. JIM 4 (1963) 1–8.
[50] J. Wang, J.M. Molina-Aldareguía, J. LLorca, Effect of Al content on the critical resolved shear stress for twin nucleation and growth in Mg alloys, Acta Mater. 188 (2020) 215–227.
[51] V. Livescu, I.J. Beyerlein, C.A. Bronkhorst, O.F. Dippo, B.G. Ndefru, L. Capolungo, H.M. Mourad, Microstructure insensitive twinning: a statistical analysis of incipient twins in high-purity titanium, Materialia 6 (2019), 100303.
[52] L. Jiang, M. Arul Kumar, I.J. Beyerlein, X. Wang, D. Zhang, C. Wu, C. Cooper, T. J. Rupert, S. Mahajan, E.J. Lavernia, J.M. Schoenung, Twin formation from a twin boundary in Mg during *in-situ* nanomechanical testing, Mater. Sci. Eng. A 759 (2019) 142–153.
[53] L. Jiang, M. Gong, J. Wang, Z. Pan, X. Wang, D. Zhang, Y.M. Wang, J. Ciston, A. M. Minor, M. Xu, X. Pan, T.J. Rupert, S. Mahajan, E.J. Lavernia, I.J. Beyerlein, J. M. Schoenung, Visualization and validation of twin nucleation and early-stage growth in magnesium, Nat. Commun. 13 (20) (2022) 1–11.
[54] C.Y. Wang, C.M. Cepeda-Jiménez, M.T. Pérez-Prado, Dislocation-particle interactions in magnesium alloys, Acta Mater. 194 (2020) 190–206.

[55] M. Lentz, R.S. Coelho, B. Camin, C. Fahrenson, N. Schaefer, S. Selve, T. Link, I. J. Beyerlein, W. Reimers, *In-situ, ex-situ* EBSD and (HR-)TEM analyses of primary, secondary and tertiary twin development in an Mg–4wt%Li alloy, Mater. Sci. Eng. A 610 (2014) 54–64.
[56] B. Leu, M. Arul Kumar, K. Xie, I.J. Beyerlein, Investigation of twin growth mechanisms in precipitate hardened AZ91, Acta Mater. 242 (2023), 118471.
[57] B. Leu, M. Arul Kumar, P.F. Rottmann, K.J. Hemker, I.J. Beyerlein, Micromechanical fields associated with irregular deformation twins in magnesium, J. Mater. Eng. Perform. (2022).
[58] S.R. Agnew, R.P. Mulay, F.J. Polesak, C.A. Calhoun, J.J. Bhattacharyya, B. Clausen, *In situ* neutron diffraction and polycrystal plasticity modeling of a Mg-Y-Nd-Zr alloy: effects of precipitation on individual deformation mechanisms, Acta Mater. 61 (2013) 3769–3780.
[59] M. Lentz, M. Klaus, M. Wagner, C. Fahrenson, I.J. Beyerlein, M. Zecevic, W. Reimers, M. Knezevic, Effect of age hardening on the deformation behavior of an Mg-Y-Nd alloy: *in-situ* X-ray diffraction and crystal plasticity modeling, Mater. Sci. Eng. A 628 (2015) 396–409.
[60] I. Basu, T. Al-Samman, Twin recrystallization mechanisms in magnesium rare earth alloys, Acta Mater. 96 (2015) 111–132.
[61] X. Ma, Q. Jiao, L.J. Kecskes, J.A. El-Awady, T.P. Weihs, Effect of basal precipitates on extension twinning and pyramidal slip: a micro-mechanical and electron microscopy study of a Mg-Al binary alloy, Acta Mater. 189 (2020) 35–46.
[62] B. Leu, M. Arul Kumar, I.J. Beyerlein, The effects of basal and prismatic precipitates on deformation twinning in AZ91 magnesium alloy, in V.M. Miller, P. Maier, J.B. Jordon et al. (eds), Magnesium Technology 2021, The Minerals, Metals & Materials Series, Springer.
[63] B. Leu, M. Arul Kumar, K.Y. Xie, I.J. Beyerlein, Twinning pathways enabled by precipitates in AZ91, Materialia 21 (2022), 101292.
[64] C. Liu, H. Chen, M. Song, J.F. Nie, Ordered Sn distribution adjacent to the precipitate-matrix interface in a Mg–9.8 wt%Sn alloy, J. Mag. Alloys 10 (2022) 1090–1914.
[65] Y. Paudel, D. Giri, M.W. Priddy, C.D. Barrett, K. Inal, M.A. Tschopp, H. Rhee, H. El-Kadiri, A review on capturing twin nucleation in crystal plasticity for hexagonal metals, Metals 11 (2021) 1373–1426. Basel.
[66] J. Wang, I. Beyerlein, C. Tomé, An atomic and probabilistic perspective on twin nucleation in Mg, Scr. Mater. 63 (2010) 741–746.
[67] D. Giri, Probing site-specific twin nucleation in hexagonal closed packed (HCP) materials with nudged elastic band (NEB) method, PhD Thesis, Mississippi State University, Starkville, MS, USA, 2020.